Biophysical Journal
Article

Biophysical Society

Positional Isomers of a Non-Nucleoside Substrate Differentially Affect Myosin Function

Mike Woodward,[1] Eric Ostrander,[2] Seung P. Jeong,[2] Xiarong Liu,[3] Brent Scott,[1] Matt Unger,[1] Jianhan Chen,[3] Dhandapani Venkataraman,[2] and Edward P. Debold[1,*]

[1]Department of Kinesiology, Muscle Biophysics Lab, [2]Department of Chemistry, Advanced Laboratory for Iontronic, Electronic and Nanomaterials, and [3]Department of Chemistry, Computational Biophysics and Biomaterials Group, University of Massachusetts Amherst, Amherst, Massachusetts

ABSTRACT Molecular motors have evolved to transduce chemical energy from ATP into mechanical work to drive essential cellular processes, from muscle contraction to vesicular transport. Dysfunction of these motors is a root cause of many pathologies necessitating the need for intrinsic control over molecular motor function. Herein, we demonstrate that positional isomerism can be used as a simple and powerful tool to control the molecular motor of muscle, myosin. Using three isomers of a synthetic non-nucleoside triphosphate, we demonstrate that myosin's force- and motion-generating capacity can be dramatically altered at both the ensemble and single-molecule levels. By correlating our experimental results with computation, we show that each isomer exerts intrinsic control by affecting distinct steps in myosin's mechanochemical cycle. Our studies demonstrate that subtle variations in the structure of an abiotic energy source can be used to control the force and motility of myosin without altering myosin's structure.

SIGNIFICANCE Molecular motors transduce chemical energy from ATP into the mechanical work inside a cell, powering everything from muscle contraction to vesicular transport. Although ATP is the preferred source of energy, there is growing interest in developing alternative sources of energy to gain control over molecular motors. We synthesized a series of synthetic compounds to serve as alternative energy sources for muscle myosin. Myosin was able to use this energy source to generate force and velocity, and by using different isomers of this compound we were able to modulate, and even inhibit, the activity of myosin. This suggests that changing the isomer of the substrate could provide a simple, yet powerful, approach to gain control over molecular motor function.

INTRODUCTION

Molecular motors, such as muscle myosin, have evolved to transduce chemical energy from the gamma-phosphate bond in ATP into mechanical work. This energy is used to power a myriad of intracellular processes, from muscle contraction (1) to the transport of organelles (2) to cytokinesis (3). Although ATP is the preferred source of molecular motors, there is growing interest in developing alternative energy sources to control biological motors and thereby control the processes they drive inside the cell (4,5). For example, the ability to preferentially inhibit the activity of skeletal muscle myosin could aid in the treatment of muscle spasticity that is so prevalent in conditions like cerebral palsy. It would also be advantageous to activate or enhance skeletal muscle myosin function in disorders in which neural input to the muscle is compromised, such as multiple sclerosis, ALS (amyotrophic lateral sclerosis), and the "easy muscle fatigue" experienced by individuals with chronic heart failure. Directly enhancing cardiac myosin function would also be a powerful approach to improve the cardiac contractility in individuals with chronic heart failure. In fact, this approach is currently being pursued using 2-deoxy ATP, an analog of ATP (6–8). Thus, gaining control over molecular motors represents a promising area for novel therapeutic approaches to treat many prevalent conditions. Gaining control over molecular motors is also a focus of nanotechnology efforts that aim to build synthetic controllable molecular motor-based nanomachines (9–13). Indeed, biological motors have even been used, in this context, to perform parallel computing tasks (14), in which precise control over the motors is critical to proper function of the nanodevice. Thus, there is growing interest in the ability to control molecular motor function both in vivo and

Submitted December 17, 2019, and accepted for publication June 17, 2020.

*Correspondence: edebold@kin.umass.edu

Mike Woodward and Eric Ostrander contributed equally to this work.

Editor: Steven Rosenfeld.

https://doi.org/10.1016/j.bpj.2020.06.024

in vitro because of the broad and powerful potential that such control would offer to both clinicians and bioengineers.

Several different strategies have been employed to gain control over the activation, speed, and directionality of molecular motors. Initial efforts using "caged ATP" enabled researchers to precisely control the initiation of contraction in muscle, providing novel mechanistic insight into the timing and sequence of the initial events of contraction (15). However, the degree of control with these types of compounds was limited to modulating the binding of the substrate to myosin's active site, creating an irreversible "on-off switch." Greater control can be gained by manipulating the surface chemistry of the experimental chamber in in vitro motility assays with isolated proteins. This strategy can be used to directly control both the pattern and speed of the filament motion driven by molecular motors (16). A related approach is to apply an external load to the charged actin filament by imposing a weak electrical field to the bathing solution in an in vitro motility assay (17). Using this approach, the velocity of the actin filament can be accelerated or decelerated by taking advantage of the load-dependent nature of myosin function (18,19).

Alternatively, the structure of the motor can be altered using molecular biology techniques to introduce new structural elements to exert control. Using this approach, the structure of myosin's motor domain can be altered such that its preferred direction of motion can be permanently reversed (20). Similar approaches have been used to incorporate photosensitive structural elements into the motor domain of myosin and kinesin that enable direct control over activation and direction of travel, which can be gated by light, with either ultraviolet (UV) (21) or blue light (11). Although these approaches demonstrate an effective means of gaining control over motor function, they are more applicable to the development of in vitro nanodevices than to a clinical setting because the structural manipulations are too severe to be successfully implemented in vivo.

An alternative approach is to manipulate the substrate to gain control over myosin. Indeed, structural analogs of ATP have been used to trap or stall myosin in otherwise transient states of the cross-bridge cycle (22). For example, nonhydrolyzable analogs of ATP such as AMPPNP and ATPγS (23) can trap myosin an ATP-bound state off of actin, and ADP complexed with aluminum fluoride (MgADP-AIF$_4$) can trap the posthydrolysis state (24). These analogs proved invaluable in generating high resolution structures of myosin in different biochemical states. However, because the purpose was to stall the motor in individual mechanochemical states, they are ill suited to be used for gaining control over functional properties. Naturally occurring structural analogs such as GTP, CTP, ITP UTP, azaATP, and deoxyATP (*d*ATP) do offer an approach to gain control over motors because they can serve as viable substrates for myosin (23,25,26). However, only *d*ATP and CTP allow muscle and myosin to generate forces, velocities, and hydrolysis rates approaching the values observed with ATP (25,27,28). Furthermore, because their structure is so similar to ATP, they offer only minor insight into the fundamental mechanisms of the energy transduction process. More important for the prospect of control, these substrates do not contain the elements necessary to gain control via an external trigger such as light.

A more powerful and versatile approach to control molecular motors in an in vivo setting is to custom design an alternative energy source (i.e., a non-nucleoside triphosphate) so that the activity of molecular motor could be controlled independent of its biological activation process. With this goal in mind, Menezes et al. (5) synthesized a triphosphate moiety onto the photoswitchable molecule azobenzene. Using this compound, myosin's velocity could be regulated with exposure to different wavelengths of light in an in vitro motility assay (5). The bulky *cis* form of azobenzene-based non-nucleoside triphosphate (AzoTP) (which predominates in UV light) likely renders AzoTP unable to bind to myosin's nucleotide binding site, whereas the flatter *trans* form (which predominates with visible light exposure) readily binds to the active site, much like ATP (5). Thus, this approach creates a type of control that is similar to that of the light-sensitive caged-ATP compounds (15), an on-off switch, or earlier photoaffinity analogs (29,30) but has the additional advantage of being reversible. However, the control over contraction is less precise than caged ATP because conversion from the *cis* to *trans* form of AzoTP is incomplete; indeed, even with prolonged exposure to UV, 5–10% of the AzoTP remains in the *trans* form, such that myosin function cannot be fully stopped. A further drawback for in vivo applications is that it would be difficult to implement an external light trigger in subcutaneous body tissues such as skeletal and cardiac muscle. Therefore, there is now a need to gain more precise intrinsic control over molecular motors, in which the substrate is modified to alter specific transitions within the molecular motor's mechanochemical cycle (i.e., the cross-bridge cycle in myosin). This would provide a substantially greater degree of control over the motor such that both the activation and the speed of the motor could be precisely modulated rather than simply turning it on and off by affecting binding to the active site.

Gaining intrinsic control over molecular motors using alternative substrates requires a detailed mechanistic understanding of how myosin uses these compounds to generate force and motion. For example, despite the fact that substrates can be used by myosin to generate motion, it is not clear how they bind to and interact with myosin's active site. It is also unclear which step or steps in myosin's mechanochemical cycle might be altered to gain control over its function. Achieving this level of knowledge requires a biophysical characterization of myosin's mechanics and kinetics at both the ensemble and single-molecule levels.

Herein, we report that myosin can use a synthetic AzoTP as an alternative energy source to generate force, as well as velocity, in in vitro assays. We show that myosin's function is profoundly sensitive to the position of the triphosphate moiety (i.e., positional isomers) on the base of the synthetic substrate.

In fact, with one isomer, myosin was able to generate ~65% of the velocity elicited when ATP is the energy source, whereas another isomer reduced myosin's velocity by ~99%, and a third isomer inhibited myosin function in the presence of ATP in a dose-dependent manner. We used a series of biophysical experiments, including single-molecule laser trap assays, to reveal how myosin used each of these AzoTP isomers to transduce energy and compared the results with those using ATP. The results demonstrate that subtle structural changes to a synthetic substrate can dramatically alter and thus control myosin's function by affecting the intrinsic properties of its mechanochemical cycle. Thus, positional isomerism provides a powerful new approach to gain control over molecular motor function and may also provide novel mechanistic insights into the fundamental nature and efficiency of energy transduction by this prototypical molecular motor.

MATERIALS AND METHODS

Chemical synthesis

AzoTP compounds (Fig. 1 *a*) were synthesized based on a protocol reported previously (5). Briefly, we added di-tert-butyl *N,N*-diisopropylphosphoramidite, followed by oxidation with *m*-chloroperoxybenzoic acid to the ortho, meta, or para isomers of hydroxy-2-ethoxy azobenzene (from here forward referred to as AzoTP) in dry tetrahydofur to form the *tert*-butyl protected monophosphate ester. The ester was deprotected with trifluoroacetic acid and was purified by eluting through a DEAE A-25 anion exchange column. During this process, the cation was converted to a triethylammonium salt. A solution of triethylammonium monophosphate salt of the azobenzene was converted to a tributyl ammonium salt by the addition of tributylamine. This monophosphate was coupled with tributylammonium pyrophosphate to obtain tributylammonium salt of azotriphosphate. This was converted to its sodium salt using sodium iodide. The synthetic procedure of each compound is provided in Fig. S1. We determined the ratio of *cis*/*trans* for each isoform of the compound and found the form used was almost exclusively in the *trans* form (>93%), as determined by H-NMR (Fig. S1 *b*).

In vitro functional assays

Proteins

Myosin and actin used in all the experiments were purified from chicken pectoralis muscle as previously described (31), with minor modifications as detailed previously (32). Roughly >95% of the myosin in this tissue is composed on the fast type IIb myosin heavy chain isoform (33). The actin was isolated as G-actin but then repolymerized and labeled with 100% tetramethylrhodamine (TRITC)/phalloidin for the in vitro motility assay and with 50% TRITC/phalloidin and 50% biotin/phalloidin for the laser trap assay experiments. All animal tissue was obtained in accordance with the policies of the National Institute of Health, using a protocol approved by the Institutional Animal Care and Use Committee at the University of Massachusetts Amherst.

In vitro motility assay

The in vitro motility assay was performed as previously described (34), with minor modifications. Briefly, myosin was loaded onto a nitrocellulose-coated coverslip surface at a saturating concentration of 100 μg/mL. The surface was then blocked with bovine serum albumin for 1 min, and unlabeled filamentous actin was added to prevent any rigor myosin molecules (aka deadheads) from slowing the labeled actin velocity. TRITC-labeled actin was then added in the absence of ATP. The final buffer was added, containing 2 mM ATP, 2 mM of an AzoTP compound, or a combination of 2 mM ATP and 2 mM of an AzoTP compound. Filament motion was visualized using a Nikon Ti-U inverted microscope (Nikon, Tokyo, Japan), with a 100×, 1.4 numerical aperture CFI Plan Apo oil-coupled objective with the temperature maintained at 30.0°C for all experiments. For each flow cell, three 30 s videos were captured at 10 frames s^{-1} and at three different locations within each flow cell.

To estimate the effect on myosin's duty ratio, i.e., fraction of its ATPase cycle spent strongly bound to actin, the surface density in the motility assay was systematically varied as previously described (35). By fitting the plot of the number of heads per filament versus filament velocity, an estimate of the duty ratio was obtained using the following equation:

$$V_{actin} = V_{max} \times \left[1 - (1 - f)^N\right],$$

where V_{max} is the V_{actin} at saturating myosin head density, N the number of myosin heads in contact with an actin filament, and f the duty ratio, which is the free parameter determined by the fit. The equation was fit to the data and visualized using the "*drc*" and "*ggplot2*" packages (36,37) in R. Fit parameters were tested for significance by calculating the difference in means.

ATPase assay

The ability of myosin to hydrolyze ATP and the ortho isomer of AzoTP was determined in solution using a malachite green assay, performed as previously described (38) with minor modifications. Briefly, the whole skeletal muscle myosin was proteolytically digested with α-chymotrypsin to make heavy meromyosin. This was purified from the light meromyosin fragments and other fragments and then dialyzed into a low-salt buffer (20 mM KCl, 25 mM imidazole, 1 mM EGTA, 4 mM $MgCl_2$, 1 mM dithiothreitol). On the day of an experiment, the heavy meromyosin was diluted to 100–400 nM and was extensively mixed with actin (10 μM) at increasing ATP concentrations for specific durations before quenching the reaction with hydrochloric acid in a 96-well plate. Absorbance was measured at 650 nm using a spectrophotometer, and a standard curve from 0 to 1.2 mM P_i was used to quantify the rate of P_i appearance. Data were fitted with a Michaelis-Menten relationship to determine V_{max} and K_M for each substrate.

Analysis of in vitro motility data

The velocity of the actin filaments as well as the percent of filaments moving was determined using an automated filament-tracking ImageJ plugin WRMTRK. Filaments shorter than 0.5 μm were eliminated from the analysis, and filaments with velocities less than 0.13 $\mu m \cdot s^{-1}$ were considered to be stationary. A typical field of view generated 25–50 filament velocities, and the mean of these velocities was taken as the average velocity for that field of view, with a total of three recordings done for each flow cell. For each condition tested, at least three flow cells were used to generate the data, resulting in at least nine recordings contributing to the overall mean filament velocity for each condition.

Single-molecule and miniensemble laser trap assays

The laser trap assays were performed at 25°C as previously described (39), and the system was calibrated with established methods (40). Myosin was loaded into a flow cell with number 1 thickness, nitrocellulose-coated coverglass (Thermo Fisher Scientific, Waltham, MA) in a high-salt buffer (300 mM KCl, 25 mM imidazole, 1 mM EGTA, 4 mM $MgCl_2$, 1 mM dithiothreitol). For single-molecule experiments, myosin was loaded at 0.05 $\mu g \cdot mL^{-1}$, but for miniensemble experiments, it was increased to 25 $\mu g \cdot mL^{-1}$. The surface was then blocked with bovine serum albumin (0.5 mg/mL) before a low-salt experimental buffer (25 mM KCl, 25 mM imidazole, 1 mM EGTA, 4 mM

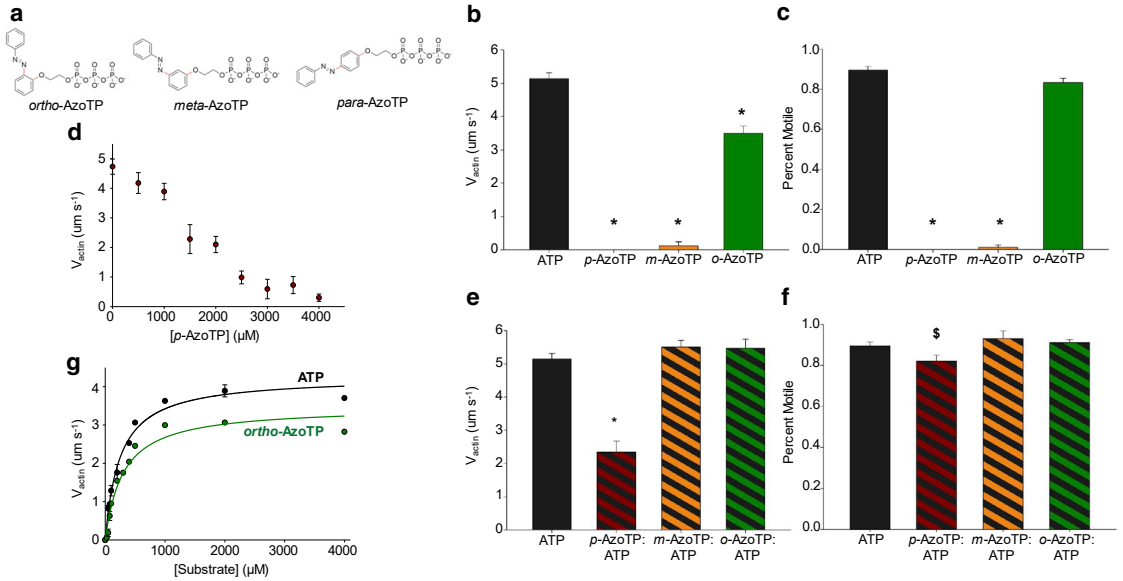

FIGURE 1 Effect of AzoTP isomers on myosin's unloaded velocity. (*a*) Chemical structures of isomers of AzoTP used in the functional assays as indicated. Note that the position of the triphosphate moiety is in the ortho, meta, or para positions on the phenyl ring in each of the three structures. (*b*) Bar graph showing the mean ± SEM of the actin filament velocities (V_{actin}) of each substrate, including a control with ATP, at a concentration of 2 mM. ATP, black ($n =$ 17 observations); para-AzoTP, red ($n = 4$); meta-AzoTP, orange ($n = 5$); ortho-AzoTP, green ($n = 11$). * indicates significantly ($p < 0.05$) different from ATP. (*c*) Mean ± SEM (standard error of the mean) for percentage of actin filaments moving in (*a*). (*d*) Mean ± SEM V_{actin}-values as a function of increasing concentrations of para-AzoTP in the presence of constant (2 mM) ATP ($n =$ 3–5 observations at each concentration of para-AzoTP, except for 2000 μM, which was more ($n = 14$)). (*e*) Mean ± SEM V_{actin}-values in the presence of mixtures of ATP and AzoTP isomers (2 mM/2 mM, respectively) as indicated; solid black bar indicates ATP control, and stripped bars indicate V_{actin}-values for compound mixtures ($n =$ 5–8 for para-AzoTP/ATP, meta-AzoTP/ATP, and ortho-AzoTP/ATP). (*f*) Mean ± SEM for percentage of actin filaments moving in (*e*); $ indicates significantly different from the meta-AzoTP value. (*g*) V_{actin} as a function of substrate concentration. Mean ± SEM V_{actin}-values for ATP (*black dots*) and ortho-AzoTP (*green dots*). Substrate concentrations ranged from 50 to 4000 μM. Each point represents one to two observations. Points fit to a Michaelis-Menten relationship, with $V_{actin} = V_{max} \times [S]/K_M + [S]$ yielding values for the maximal velocity ($V_{max} = 4.3 \pm 0.14$ and 3.5 ± 0.22 $\mu m \cdot s^{-1}$ for ATP and ortho-AzoTP, respectively) and the substrate concentration that produced one half of the maximal velocity ($K_{1/2} = 244 \pm 25$ and 298 ± 54 μM for ATP and ortho-AzoTP, respectively). Both V_{max} and $k_{1/2}$ were significantly ($p < 0.05$) different between ATP and ortho-AzoTP. To see this figure in color, go online.

$MgCl_2$) with appropriate concentration of ATP or AzoTP. The experimental buffer also contained 1-μm-diameter silica beads (Bangs Laboratories, Fishers, IN) coated with neutravidin, providing a linkage for attachment to the biotin/TRITC-labeled actin filaments. Two of these 1 μm neutravidin-coated silica beads were trapped in time-shared laser traps, and a single TRITC/biotin-coated actin filament was attached to both beads in a three-bead configuration previously detailed (41). Compliance of this bead-actin-bead assembly was minimized by applying 3–4 pN of pretension, and the laser power set was such that the combined trap stiffness of the dumbbell was 0.02 pN per nanometer, which was determined based on the Brownian motion of the bead-actin-bead assembly when not attached to myosin using equipartition theory (42). The dumbbell was then brought into contact with the myosin head(s) on the surface by approaching the nitrocellulose-coated 3 μm silica bead.

Analysis of laser trap assay data

To determine the size of myosin's powerstroke (*d*) and the duration of actomyosin strong binding (t_{on}), the raw actin displacement data were analyzed using a mean-variance analysis as previously described (43). Briefly, the mean and variance of the raw displacement records were calculated within a defined time window (e.g., 30 ms). This window was advanced over the entire displacement record, and the calculated mean and variance within each window was plotted in a three-dimensional histogram with the third dimension indicating the number of observations binned within a specific mean-variance value. Myosin's step size was taken as the distance in nanometers from the center of the fit to the unbound lifetime (baseline, *B*) and the center of the event population (*e*).

Varying the window width over a single displacement record provides a measure of the density of binding events at each window width. Event density (*p*) as a function of the window width (*tw*) was then plotted and fitted with a monoexponential decay, with t_{on} the amount of time myosin spends strongly bound to actin and *N* the number of binding events, using the following equation:

$$p(tw) = ton \times Ne^{(1-tw)/ton}.$$

A separate custom analysis program was used to analyze the miniensemble laser trap assay data to determine peak force and event duration for all recordings. This threshold-based program was similar to the method we previously published (44) with minor modifications, including automated detection (39). Briefly, the data were processed with a custom Python script to correct for baseline wander. Analysis of the processed data, including the event detection and measurements, was completed in R 3.5.2 (45) using custom programs with functions from the "*tidyverse*" and "*gtools*" packages (37). Briefly, the baseline corrected data was low-pass filtered using a running mean with a 10 ms (50 data points, at the sampling rate of 5 kHz) window width, and the events were identified using two criteria: 1) a +8 nm threshold was set to the running mean to signal the start or end of an event, and 2) the event was included in further analysis if the duration was greater than 10 ms. Event durations were calculated as the time between the start or end (8 nm) thresholds, and the time-off measurements were calculated as the time between the end of an event and the start of the subsequent event. Peak forces were calculated by identifying the maximal displacement of each record and converting the displacement in

nanometers to forces in pN (0.04 pN • nm^{-1}). Plots of the raw data and representative analysis traces were constructed using the "*ggplot2*" and "*cowplot*" R packages (37,46). The data were then plotted in a histogram (Fig. 3 *b*) and the arithmetic means reported (Fig. 3, *d–f*).

Molecular modeling and dynamics simulations

Atomistic simulations of myosin in complex with ATP or AzoTP molecules were carried out using CHARMM/OpenMM program (47,48). The latest CHARMM 36 m force field (49) was applied to model protein, water, and ions, and the CHARMM general force field (50) was used to model the small molecules. The initial protein structure was obtained from RCSB Protein Data Bank entry PDB: 1MMD (51). Coordinates of Mg^{2+} and water molecules from this PDB structure were also retained. ATP and AzoTP molecules were first generated using CHARMM-GUI (52,53). The ligand was then translated to the binding pocket of myosin, with the coordinates of TP group replaced by those of ADP•BeF_3 in PDB: 1MMD and the Azo group reoriented to mimic the binding pose of ADP. The initial structure of the myosin-ligand complex was energy minimized in vacuum for 5000 steps to remove any steric clashes. It was then placed in a rectangular simulation box containing ~28,000 TIP3P water molecules such that the minimal distance between protein surface and box edge was at least 12 Å. Nine K^+ ions were also added to neutralize the system. The simulation box was ~126 × 96 × 78 Å (49), and a periodic boundary condition was imposed for all simulations.

The solvated systems were energy minimized using steepest descent and adopted basis Newton-Raphson algorithms. Each system was then slowly heated up from 100 to 300 K in a 10 ps simulation, with the heavy atoms of protein and ligand restrained by harmonic potentials with a force constant of 5 kcal/mol/Å (48). Another 1 ns simulation was also performed to equilibrate the system at 300 K and 1 atm, with the retraining potentials slowly reduced to zero. The final production runs were carried out under the same NPT conditions without any restraint, except that the Azo group was restrained at the *trans* conformation with a harmonic potential of force constant 5 kcal/mol/Å (48). In all simulations, the nonbonded interactions were truncated at 13 Å, and long-range electrostatic interactions were treated with particle mesh Ewald method (54). Lengths of all bonds involving hydrogen atoms were constrained using the SHAKE algorithm (55). The time step to integrate the equation of motion was 2 fs, and final production runs lasted for at least 100 ns.

Additional statistical analyses

Comparisons among the single-molecule laser trap assay and motility data were determined using ANOVA and Tukey's post hoc tests (Sigmaplot 11.0) to locate differences, with the α-level set at $p < 0.05$. A Student's *t*-test was used to determine whether the ortho-AzoTP resulted in a significant difference in myosin's step size or duration of strongly bound lifetime (*t*on) versus ATP.

The nonlinear regression for estimating the xDP-release and xTP-binding rates (Fig. 5) were performed in *R* version 3.5.2 using the *nls* function from the "*stats*" package (45), which optimizes the fit using the least squares method (Gauss-Newton algorithm). Summary statistics from the regression were extracted using the *tidy* function from the "*broom*" package (56). These data were visualized using the "*ggplot2*" package (37). The goodness of fit for regression was determined through the residual plots using the *nlsResiduals* function in the "*nlstools*" package (57).

RESULTS

Positional isomers of AzoTP differentially affect myosin function

We synthesized three positional isomers of AzoTP to use as non-nucleoside energy sources for fast skeletal muscle myosin. >93% of the compound was confirmed to be in the *trans* form based on mass spectrometry measurements (see Fig. S1). The phosphate moiety was placed at the ortho, meta, or para positions of one of the phenyl rings (Fig. 1). Each compound was tested to determine its ability to power muscle myosin as it translocated actin filaments in an in vitro motility assay (Fig. 1 *b*). The velocity of the actin filaments in the motility assay (V_{actin}) was determined and compared with the value observed when ATP served as the control substrate (Fig. 1 *b*). When para-AzoTP was used as the energy source, myosin did not move the actin filaments (Video S1), suggesting it cannot harness the energy in the triphosphate. Likewise, no filament motion was initially observed when using meta-AzoTP; however, upon closer examination over a more extended timescale (2 min vs. 30 s), there was clear evidence of actin filament motion with meta-AzoTP, albeit with an extremely slow velocity of 70 nm s^{-1}, less than 1% of the velocity observed with ATP (Video S2). Indeed, almost all of the filaments (~90%) moved at a constant velocity of 70 nm s^{-1}, suggesting that myosin is still using the energy of meta-AzoTP but that one or more steps in its mechanochemical cycle was drastically slowed. In contrast to the para and meta isomers, with ortho-AzoTP serving as the energy source, myosin generated a V_{actin} that was ~65% of that observed using ATP (Fig. 1 *a*; Video S3), and as with ATP, >80% of the filaments were motile (Fig. 1 *c*). These findings demonstrate that myosin can harness the energy from a non-nucleoside triphosphate to power actin filament motion.

50/50 mixtures of each AzoTP variant with ATP were investigated to determine whether the compounds could inhibit myosin function in the presence of ATP. When meta- or ortho-AzoTP were mixed with equal amounts of ATP, V_{actin} was similar to ATP alone, suggesting that they do not affect myosin's interaction with ATP and thus likely do not inhibit myosin function (Fig. 1 *d*). In contrast, *para*-AzoTP slowed V_{actin} by 50% when it was mixed with an equal amount of ATP (2 mM) (see Videos S4A and S4B). The percentage of moving filaments in this mixture was equal to that of ATP alone (Fig. 1 *c*), suggesting that the decreased velocity was not due to an increased portion of nonmoving filaments.

To determine the nature of this inhibition, we examined the effect of para-AzoTP on V_{actin} as a function of the concentration para-AzoTP, initially at a constant ATP concentration of 2 mM (Fig. 1 *d*). This revealed a linear decrease in V_{actin} as a function of the concentration of para-AzoTP. To further delineate the mechanism of inhibition, we measured the degree of inhibition of three different para-AzoTP concentrations while varying the ATP concentration. These findings indicated that the inhibitory effect of para-AzoTP did not increase as the ATP concentration was decreased (Fig. S2), suggesting that para-AzoTP acts as an uncompetitive inhibitor of ATP (58). Importantly, the inhibitory effects were readily reversible because washing out the

para-AzoTP with a 2 mM ATP buffer almost completely restored V_{actin} to the control (ATP) value (Video S5).

The ability of myosin to use ortho-Azo-TP to generate actin filament velocities in the motility assay at 65% of the value with ATP (Fig. 1 *b*) enabled us to identify the steps in myosin's mechanochemical cycle that might be altered by the synthetic substrate. We started this effort by measuring V_{actin} as a function of the substrate concentration (Fig. 1 *g*) and found that V_{actin} was slower with ortho-AzoTP at all substrate concentrations, with the maximal velocity (V_{max}) observed to be 65% of that of the value with ATP. Notably, at low substrate concentrations (<100 $\mu\mu$M), the filaments stopped moving with ortho-AzoTP, but filament motion was detected down to 50 μM when ATP was the substrate. These data were fitted to a Michaelis-Menten relationship and indicated that the $K_{1/2}$ for ortho-AzoTP was higher than for ATP, suggesting that ortho-AzoTP may have a lower affinity for myosin's nucleotide binding site. However, the decrease in V_{actin} at saturating substrate concentrations (>1 mM) suggested that either myosin's powerstroke is decreased and/or the rate of release of the diphosphate form of the substrate was slower than with ATP (59).

Consistent with these observations, we found that myosin's steady-state ATPase rate in solution was also slowed by ~50% and that the K_M was increased by ~33% (Fig. 2, *a* and *b*). However, a motility-based assay suggested that duty ratio was not significantly changed (5 vs. 8% for ATP versus ortho-AzoTP) by the change in substrate (Fig. 2 *c*). These findings suggest that both of the kinetics steps that occur off and on actin are slowed equally when ortho-AzoTP is the substrate, at least under the unloaded conditions of this assay.

Ortho-AzoTP affects myosin's single-molecule mechanics and kinetics

To more clearly delineate the mechanism underlying the decreased V_{actin} with ortho-AzoTP versus ATP, we directly measured the size of myosin's powerstroke (i.e., step size) and the duration of actomyosin binding (t_{on}) using a single-molecule laser trap assay (Fig. 3 *a*). Compared to ATP, myosin produced a step size (7 nm) with ortho-AzoTP (Fig. 3, *b* and *c*), was statistically similar to that observed with ATP (9 nm). Strikingly, at 10 μM, the lifetime of a single actomyosin interaction (t_{on}) was nearly 10-fold longer with ortho-AzoTP versus ATP (Fig. 3 *c*). Indeed, even when the substrate concentration was increased to 50 μM, the binding event lifetimes with ortho-AzoTP remained significantly longer than those at the 10 μM ATP (Fig. 3 *c*). An equivalent measure of t_{on} at 50 μM ATP could not be obtained because binding events were shorter than the resolution of the instrument (~5–7 ms). The longer t_{on} observed in the single-molecule laser trap assay is consistent with the lower $K_{1/2}$ from the in vitro motility assay data (Fig. 1 *g*) and the slower overall AzoTPase rate (Fig. 2 *a*). Indeed, the single-molecule experiments provide much greater spatial and temporal resolution than in the bulk motility assay, in which quantifying V_{actin} at micromolar substrate concentrations can be beyond the resolution of the instrumentation. Thus, these data suggest that ortho-AzoTP either binds much more slowly to myosin in the rigor state or that ortho-AzoTP is much slower to initiate the structural events that cause myosin's dissociation from the actin filament (60). We gained further insight into the mechanism of transduction by combining the step size (*d*) determined from the single-molecule assay (Fig. 3, estimated to be 9 nm for both substrates because they were statistically indistinguishable), with the measurements of V_{actin} as a function of the substrate concentration in the motility assay (Fig. 1 *g*), using a simplified model of myosin's cross-bridge cycle (Fig. 4). This model estimates the rates of 1) the release of the diphosphate form of AzoTP (k_{-AzoDP}) from myosin and 2) the rate of AzoTP binding (k_{+AzoTP}) to myosin's active site (61). The model assumes that t_{on} is composed of the time waiting for the diphosphate form of the substrate to dissociate from myosin (*inset*, Fig. 4) and

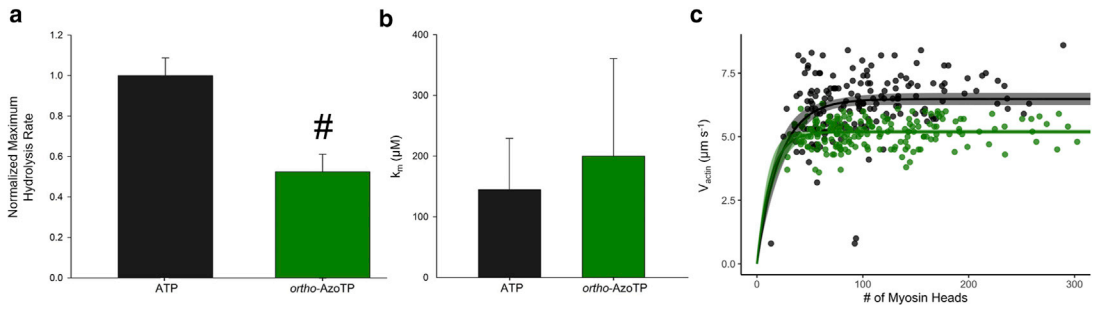

FIGURE 2 Steady-state hydrolysis rates and duty ratio estimates for ATP versus ortho-AzoTP. Myosin's steady-state hydrolysis rate uses a malachite green assay (see Fig. S3). (*a*) V_{max} ± mean ± SEM; # indicates a trend (p-value = 0.06) toward a significant difference. The hydrolysis rate was 0 in the absence of either substrate. (*b*) K_M ± SEM, which was not significantly different comparing the substrates. (*c*) Individual filament velocities plotted as a function of the filament length to estimate the effect on myosin's duty ratio (see Materials and Methods). Data fitted with $V_{actin} = V_{max} \times [1 - (1 - f)^N]$ with 95% confidence intervals revealed duty ratio estimates of 5 ± 1 and 8 ± 2%, mean ± SEM for ATP and ortho-AzoTP, respectively. 95% confidence intervals were constructed around each parameter to determine significant differenences. To see this figure in color, go online.

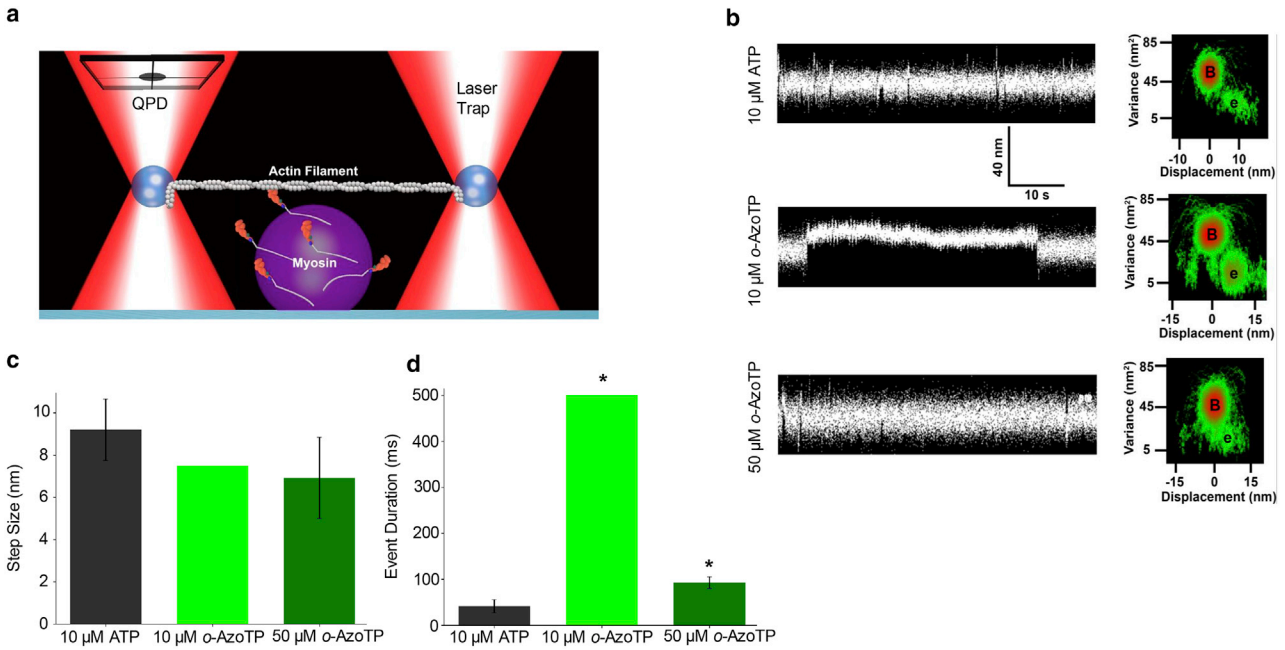

FIGURE 3 Effect of ortho-AzoTP on myosin's step size and binding event duration. (*a*) Schematic of the single-molecule laser trap assay used to determine myosin's single-molecule step size and binding event duration (see Materials and Methods). Actin filament displacement was tracked using a quadrant photodiode (QPD). (*b*) Raw actin filament displacement records from the single-molecule laser trap assay at 10 μM ATP and at 10 and 50 μM ortho-AzoTP. Actomyosin binding events are visible as reductions in the noise of the signal and a shift in the mean displacement. Binding events were much longer using ortho-AzoTP than ATP at 10 μM ATP. These data were analyzed using the mean-variance analysis (see Materials and Methods), which calculates the mean and variance within a defined window of the data (e.g., 50 ms). The window is moved over the entire record, and the results are plotted as mean displacement versus variance, with color intensity indicating the amount of time spent at each value (*red* indicates highest intensity, *green* the lowest). The resultant three-dimensional histogram of the data reveals a baseline population B corresponding to the periods when myosin is not strongly bound to actin and an event population e corresponding to periods of actomyosin strongly binding. The step size is determined as the difference between the B and e along the displacement axis. (*c*) Mean ± SEM of myosin's single-molecule step size in nm. The total number of actomyosin binding events for 10 μM ATP and 50 μM ortho-AzoTP were $n = 202$ and $n = 67$, respectively. The mean step size was determined from the MV (mean variance) analysis of the data records was 9 ± 2 and 7 ± 2 nm for ATP and AzoTP, respectively. Because of the extremely long binding event durations, the total number of binding events for 10 μM AzoTP ($n = 56$) was much less than for 10 μM ATP ($n = 202$) despite a longer duration of recording time (375 and 260 s for AzoTP and ATP, respectively). (*d*) Mean ± SEM event durations at the indicated substrate concentrations. These were determined by plotting the event density as a function of window width using the mean-variance analysis (see Materials and Methods). To see this figure in color, go online.

the time waiting for the next triphosphate molecule to rebind to myosin and cause dissociation from actin. This was fitted to the motility and single-molecule data (Fig. 4) using the following equation:

$$t_{on} = (k_{-AzoDP}) + ((k_{+AzoTP})[AzoTP] / (k_{+AzoTP})[AzoTP](k_{-AzoDP})),$$

where t_{on} is the duration of strong actomyosin binding (obtained by dividing the single-molecule step size, d (9 nm) by V_{actin} at each substrate concentration (Fig. 4)), k_{-AzoDP} is the rate of release of the diphosphate form of AzoDP, k_{+AzoTP} is the second-order binding constant of AzoTP to the rigor state, and [AzoTP] is the substrate concentration.

The results of modeling indicated that k_{+AzoTP} was ~50% slower for ortho-AzoTP than for ATP (Fig. 4), consistent with a lower $K_{1/2}$ from the Michaelis-Menten fit to the V_{actin} data (Fig. 1 *g*) and lower Km in the steady-state ATPase data (Fig. 2 *b*). The model also suggests that myosin released AzoDP ~20% slower than ADP (Fig. 4). These findings suggest that the slower V_{actin} at low ATP is due to a slower rate of AzoTP binding to, and dissociating myosin from, the actomyosin rigor complex, whereas at saturating substrate levels, the slow rate of ortho-AzoDP drives the slower V_{actin}. Indeed, the substrate-induced dissociation was so much slower at 10 and 50 μM that these data points could not be fitted by the model (data not shown), suggesting that k_{+AzoTP} may be even slower than our model estimate.

Myosin can harness the energy in ortho-AzoTP to generate force

To gain a more complete assessment of myosin's ability to transduce energy from a synthetic energy source, we also quantified myosin's force-generating capacity with ortho-AzoTP. This was done by using the laser trap assay as a picoNewton force transducer, in which force is generated by a miniensemble of myosin molecules (Fig. 5 *a*). Under the control condition with ATP serving as the substrate, the miniensemble of myosin molecules (~8) bound to and

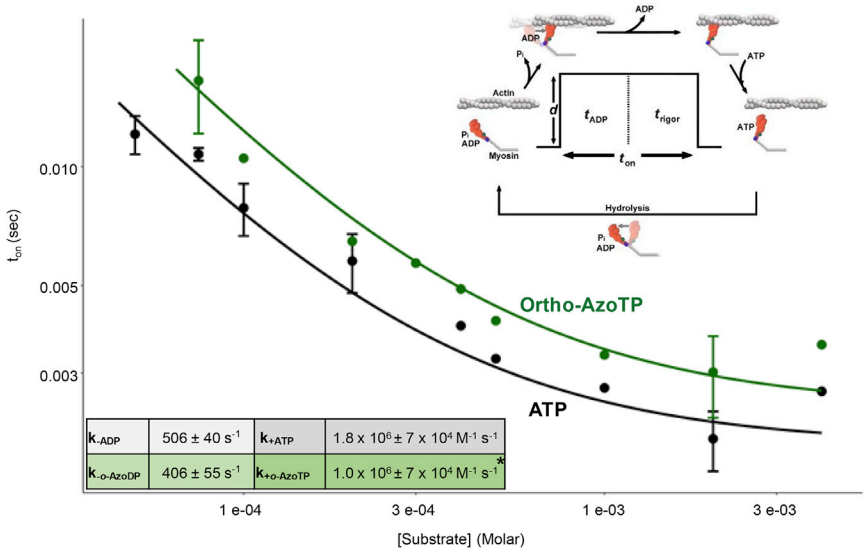

FIGURE 4 Effect of substrate concentration of myosin's kinetics and mechanics. The main graph shows calculated or measured actomyosin event durations plotted as a function of substrate concentration for ATP (*black*) and ortho-AzoTP (*green*). Event durations (t_{on}) from 4 mM down to 75 μM were determined by dividing the single-molecule step size of 9 nm (Fig. 3 *c*) by V_{actin} at the corresponding substrate concentration in the motility assay (see Fig. 1). Data points represent mean ± SEM. The data were fitted to an equation (see Materials and Methods) based on a simple model of myosin's cross-bridge cycle (*inset figure*). The fit yielded values for the rate of the second-order xTP-induced binding constant (k_{+ATP} and k_{+AzoTP}). The value for k_{+AzoTP} was significantly ($p < 0.05$) slower that for k_{+ATP}, indicated by * in the inset table. The fit indicated that the rate of xDP release (k_{-AzoDP}) was not significantly faster for AzoTP. Parameter estimates were tested for significance using an F-test. To see this figure in color, go online.

translocated the actin filament against the spring-like load of the laser trap (Fig. 5 *b*). The stochastic nature of myosin binding and unbinding to the actin filament causes a distribution of forces to be generated, with peak forces ranging from 0.2 to 3.5 pN and an average force equal to 1 pN (Fig. 5 *c*).

In the presence of ortho-AzoTP, myosin was able to generate roughly 65% of the force observed with ATP (Fig. 5 *b*). Representative raw records show that the runs of motility of these ensembles were shorter than with ATP (Fig. 5 *b*), despite the experiments being performed with the same number of myosin molecules and the same trap stiffness. A full analysis of all binding events revealed a reduction in the number and amplitude of force-generating events (Fig. 5 *c*), resulting in 35% less peak force than with ATP (Fig. 5 *d*). Consistent with the reduction in force, the average lifetime of the binding events was reduced by roughly the same amount as the force (38%; Fig. 5 *d*). This suggests that the drop in force, relative to ATP, is due to a slowed rate of attachment of myosin heads to the actin filament; the longer time between binding events adds further support for this hypothesis (Fig. 5 *e*). Despite the reduced force levels, these data do demonstrate that this variant of a non-nucleoside synthetic triphosphate compound can be used by myosin to generate force over a distance, and thus mechanical work, in addition to its ability to propel actin filaments (Fig. 1 *b*).

Similar force measurements could not be made using para-AzoTP because myosin did not generate any movement when it was used as a substrate (Fig. 1 *b*). Likewise, the extremely slow velocity generated when meta-AzoTP was the substrate (~1% of that with ATP) prohibited the ability to accurately measure the force-generating capacity with this substrate.

DISCUSSION

We successfully demonstrated that myosin can transduce chemical energy from a photoswitchable, non-nucleotide triphosphate compound into mechanical work (Figs. 1 and 5). Furthermore, by changing only the position of the triphosphate moiety from the ortho to para positions, AzoTP can be transformed from an energy source into an inhibitor of myosin function in the presence of its preferred energy source, ATP. In addition, by moving the triphosphate moiety to the meta position, myosin function can be slowed to <1% of the ATP-driven velocity. Thus, we have demonstrated that myosin's force- and motion-generating capacity can be intrinsically controlled using a non-nucleoside-based molecule, enabling us to "shift the gears" of this molecular motor. Furthermore, by manipulating the substrate concentration and changing the number of myosin molecules in the assays, we have gained insight into the mechanisms underlying this control over the motor's "transmission."

Previous reports of using light-sensitive compounds to power muscle myosin found that specific variants of AzoTP can generate actin filament velocities up to 70% of ATP (5,62). However, only molecules with the triphosphate moiety in the ortho position were examined and only under unloaded conditions (e.g., in vitro motility assay or ATPase), in which no external work is performed by the motor. Therefore, our use of the miniensemble laser trap assay demonstrates for the first time, to our knowledge, that myosin can harness the energy from AzoTP to produce force against an external load and therefore generate mechanical work using a substrate other than its preferred source, ATP (Fig. 5). This finding provides novel, to our knowledge, insight into the mechanism of myosin's energy transduction because myosin's force-generating capacity is thought to be limited

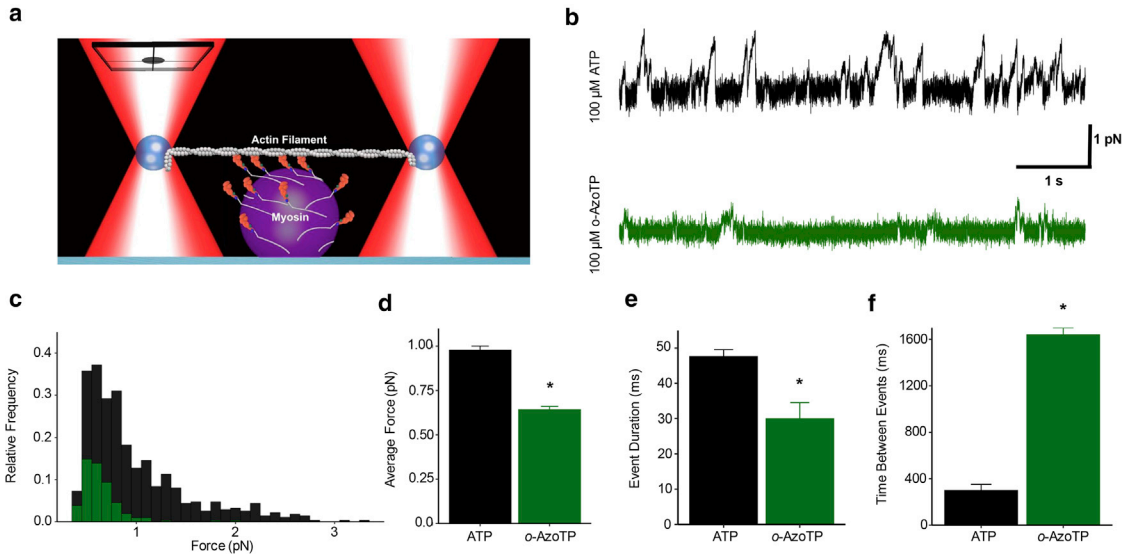

FIGURE 5 The effect of ortho-AzoTP on myosin's force-generating capacity. (*a*) A schematic of the miniensemble laser trap assay used to determine myosin's force-generating capacity. The assay is identical to the single-molecule laser trap assay (Fig. 3 *a*) except that the concentration of myosin of the surface is increased such that ~8 myosin heads are available to interact with the single actin filament and the substrate concentration was increased to 100 μM. Force was determined from the displacement records by multiplying the displacement (*d*) by the trap stiffness (i.e., force = $k_{trap} \times d$). Trap stiffness was typically 0.02 pN • nm^{-1} as determined by the equipartition method (see Materials and Methods). (*b*) Raw force records for ATP (*black*) and *ortho*-AzoTP (*green*). Multiple myosin molecules bind to the actin filament, creating runs of motility against the increasing force of the laser trap. (*c*) Peak force for each binding event was determined using a custom algorithm (see Materials and Methods) and was plotted in a histogram for each substrate. The total number of events for ATP was 692 and for ortho-AzoTP was 159, and the total amount of all data records was 274 s for ATP and 309 s for ortho-AzoTP. (*d*) Mean ± SEM peak force for each substrate. The mean forces were 0.98 ± 0.02 pN for ATP and 0.64 ± 0.02 pN for ortho-AzoTP mean ± SEM. (*e*) Binding event duration was determined by a custom algorithm (see Materials and Methods) and was 48 ± 2 ms for ATP and 30 ± 4 ms for ortho-AzoTP mean ± SEM. (*f*) The time between binding events was also calculated using our custom algorithm and was 303 ± 23 ms for ATP and 1644 ± 198 ms (mean ± SEM) for ortho-AzoTP. * indicates significantly ($p < 0.05$) different from ATP. To see this figure in color, go online.

by distinctly different mechanisms than its unloaded velocity (59,63,64). In addition, our systematic manipulation of the position of the triphosphate moiety on the azobenzene molecule offers detailed insight into how the substrate might interact with myosin's nucleotide binding site.

Ortho-AzoTP slows actomyosin dissociation rate

Although myosin was able to generate force and velocity using ortho-AzoTP, it produced significantly less than the amount it could generate using its preferred source, ATP (Figs. 3 and 5). The ~35% drop in velocity, compared with ATP, could be due to either a decrease in myosin's single-molecule step size and/or a slowing of one or more of the kinetic steps that occurs while myosin is bound to actin (59). The results of the single-molecule laser trap assay revealed slower kinetics (Fig. 5) that could explain the slower velocity. Although the effect did not reach significance, we cannot rule out that the reduced step size might also play a role in the depression of V_{actin}. Indeed, the effect on the strongly bound event lifetime was striking at 10 μM AzoTP in the single-molecule laser trap assay (Fig. 3, *b* and *d*). Even at a fivefold higher substrate concentration, myosin stayed bound to actin significantly longer than with ATP at 10 μM (Fig. 3 *d*). This is indicative of a slowed rate of the substrate binding compared with myosin's ATP-binding and/or a slower rate of dissociation of myosin from the actin filament (Figs. 3 and 5), suggesting that myosin has a weaker affinity for ortho-AzoTP than for ATP, which is consistent with the higher $K_{1/2}$ observed when measuring V_{actin} as a function of substrate concentration (Fig. 1 *g*). Although the effect did not reach significance, the modeling data suggested that the rate of release of the diphosphate form of the substrate was also slowed by ~20% compared to ATP (Fig. 4). Interestingly, the slowing of the kinetics steps occurred despite maintaining myosin's duty ratio of ~3% (Fig. 2 *c*). This suggests that most or all of the steps in the cross-bridge cycle could be slowed with this alternative substrate, which is consistent with the slowed overall xTPase rate (Fig. 2 *a*). Because the decrease in substrate binding is not limiting at saturating concentrations, this suggests that most of the reduction in V_{actin} at >1 mM is largely due to the slowed rate of ortho-AzoDP-release rate.

The decrease in myosin's force-generating capacity was similar in magnitude (Fig. 5) to the decrease in V_{actin} (Fig. 1), at roughly 65% of the value observed with ATP. Force at the molecular level is dependent on the product of the force of a single actomyosin cross-bridge and its duty ratio (i.e., the portion of its cross-bridge cycle spent strongly bound to the actin filament) (64). Therefore, the

observed 35% reduction in the peak force-generating capacity (Fig. 5) could be due to a decrease in one or both of these parameters. The dramatic decrease in the frequency of binding events, as well as the increase in time between events (Fig. 5 *f*) suggests that myosin attaches to actin more slowly in the presence of ortho-AzoTP. This is evidenced not only by lower average force but also by the reduced frequency of binding events and the absence of any high-force events (>1 pN; see Fig. 5 *c*). Myosin's attachment rate is governed by how quickly it can hydrolyze the substrate and how quickly it can go from weakly to strongly interacting with actin (65). Thus, once ortho-AzoTP binds to myosin's active site and causes dissociation from actin, it may have difficulty achieving the proper configuration to break the gamma-phosphate bond in AzoTP (60). This would cause myosin to remain dissociated from actin for a longer period of time than it would with ATP, which is consistent with the slowed overall AzoTPase rate (Fig. 2 *a*). Therefore, in comparison to myosin's cross-bridge cycle with ATP, these data suggest that at saturating ortho-AzoTP concentrations, the most pronounced effect is a slower rate of hydrolysis that greatly increases the time spent off of actin, at least in this loaded assay (Fig. 5 *c*). The steps of the cross-bridge cycle thought to be altered based on these findings are represented in the model of the cross-bridge cycle shown in Fig. 6. This finding is in contrast to the effects on the motility assay in which the duty ratio was unaffected by the change in substrate; therefore, it is possible that the substrate affects the loaded, but not unloaded, duty ratio.

Thus, despite being able to use this synthetic energy source to power force and motion, myosin is not able to harness as much of the energy as it can with ATP. This is interesting because nearly all of the contacts between myosin and ATP occur between the gamma phosphate and Mg^{2+} (66), and the synthetic energy source should thus interact with the active site in a manner similar to ATP and possess nearly the same free energy because it comes from the breakage of the same gamma-phosphate bond. Therefore, the observed altered function suggests that the base portion of ATP must also play a role in proper binding of the substrate to the active site, as well as the efficiency of energy transduction. Indeed, simply rotating the position of the triphosphate moiety on the phenyl ring profoundly impacted myosin function (Fig. 1). These findings share some similarities with nucleoside-based analogs (23,25,26); however, these may be coincidental given that

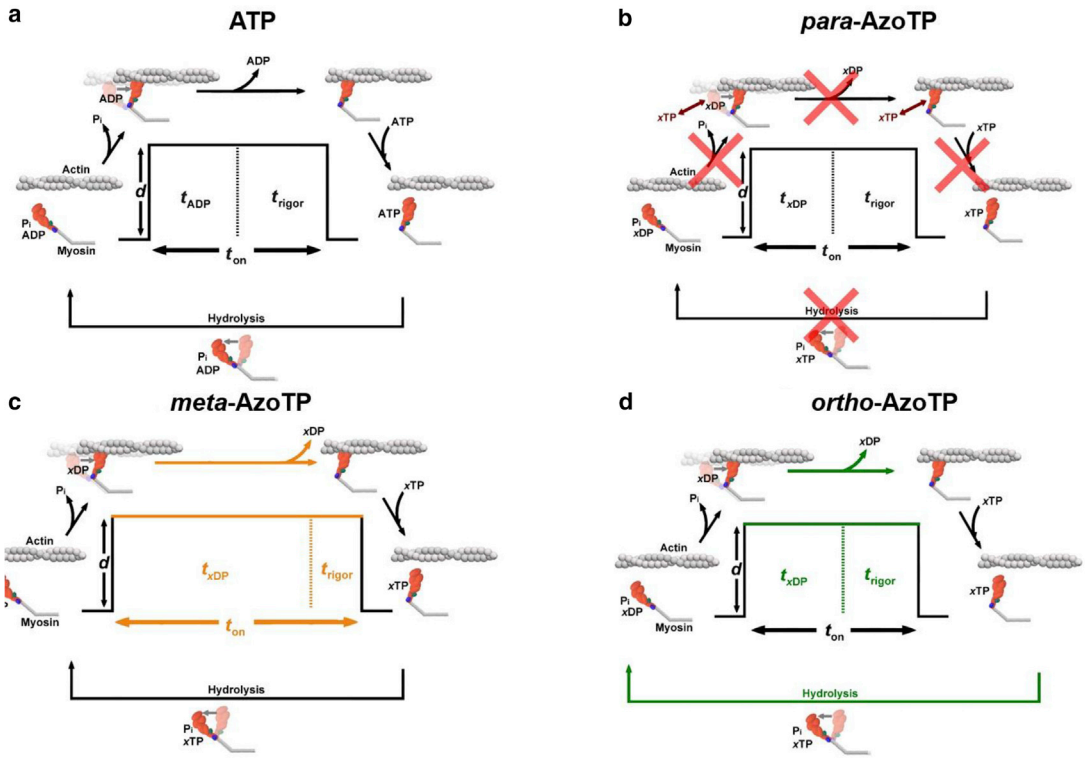

FIGURE 6 Hypothesized schemes of how each isomer affects myosin's cross-bridge cycle. (*a*) A simplified model for the cross-bridge cycle with ATP. (*b*) para-AzoTP traps filaments in a what appears to be a rigor-bound state (see Video S1), suggesting that para-AzoTP binds to actomyosin in the rigor state and prevents the release of the diphosphate form of the compound or that para-AzoTP does not bind to the active site. We favor the latter because the mechanism of inhibition appears to be uncompetitive (see Fig. S5). The transitions marked with a red "X" are unlikely to occur. (*c*) For meta-AzoTP, the slowed velocity at saturating substrate concentrations (Fig. 1 *b*) suggests that it was not due to a decrease in the percentage of moving filaments (Video S2 versus Video S7), suggesting that the diphosphate form of the substrate is released more slowly than ADP. This idea is depicted as a prolonged xDP lifetime. (*d*) Ortho-AzoTP was used by myosin to generate force and motion but has a prolonged rigor lifetime at low substrate concentration and maybe a slower rate of AzoDP-release (Fig. 4), and at least one step off of actin is slowed because it generates ~35% less force than with ATP (Fig. 5). To see this figure in color, go online.

the structure of the base portion of the substrate in this study is not a nucleoside.

To directly examine the nature of the interactions between the substrate and myosin, we performed molecular dynamics simulations in which the substrate was docked in the active site, and the nature of the interactions between myosin's ATP-binding site and each substrate were qualitatively determined. In general, these simulations show that the ortho version of AzoTP maintains a binding pose in the active site that is quite similar to ATP (Videos S6A, S6B, S6C, and S6D), providing potential insight into why it is a much better substrate for myosin than either the para or meta versions of AzoTP. Thus, the 35% decrease in force and velocity observed with ortho-AzoTP may be due to the subtle variations in its interactions with myosin.

Para-AzoTP is an uncompetitive inhibitor of ATP

In contrast to the relatively high efficiency of energy transduction observed using the ortho form of AzoTP, myosin did not move in the presence of the para isomer of AzoTP (Fig. 1). Interestingly, when mixed with ATP in the motility assay, the para variant of AzoTP inhibited myosin function in a dose-dependent manner (Fig. 1 *d*), reducing velocity by 50% when both substrates were set to an equal concentration of 2 mM. The inhibition was readily reversible (Video S5); however, it was less pronounced at lower ATP concentrations (Fig. S2) than would be expected with a competitive inhibition mechanism (67). Indeed, the data are most consistent with an uncompetitive or anticompetitive mechanism (67), in which the inhibitor recognizes and traps the enzyme substrate complex, creating a branch in the canonical pathway (68). With this type of inhibition, the effect is only dependent on the concentration of the inhibitor and not the ATP concentration (68), and thus, the inhibition is not reversed by increasing the substrate concentration (in this case, ATP) (68). There are previous reports of uncompetitive inhibitors of myosin (69–71); however, they typically act to prevent actomyosin binding (e.g., blebbistatin (71)) and, as a consequence, actin-induced acceleration of P_i release from the active site, trapping myosin in an unbound or weakly bound state (72). In this study, actin filaments in the presence of para-AzoTP and ATP still move at a very slow velocity, even at saturating para-AzoTP concentrations, suggesting that it does not compete with ATP but inhibits product release on actin (e.g., ADP release) and/or slows ATP-induced dissociation from actin. This is an important finding because the ability to inhibit myosin is a very powerful tool in biology, but most inhibitors inhibit P_i release or actin binding (72); therefore, this compound would provide researchers with a new, to our knowledge, inhibitor to more precisely characterize different mechanisms of cellular processes driven by myosin. The reversibility of the compound also presents an advantage over other compounds such as blebbistatin, which are typically nonreversible (73).

Our molecular dynamics simulations with this compound were initiated with para-AzoTP in the active site, which may be a rare event in the in vitro motility assay but nonetheless shows that the triphosphate moiety can fit into myosin's ATP-binding site. However, the simulations also indicate that this phenyl ring makes strong contact with a tyrosine residue near the ATP-binding site and can lead to significant deformation of the loop (Videos S6A, S6B, S6C, and S6D). Thus, it is somewhat surprising that despite being a triphosphate compound, it does not appear to competitively inhibit myosin. One possible mechanism of action to explain this discrepancy is that para-AzoTP recognizes when myosin has a nucleotide in the active site (ADP or ATP) and traps myosin in the actin-bound state as an uncompetitive inhibitor (see Fig. 6).

Meta-AzoTP greatly slows myosin's velocity

Myosin's mechanochemical cycle seems to be altered in a distinctly different way when meta-AzoTP is the substrate. Myosin moves actin but at only ~1% of the velocity of ATP, despite all the filaments moving in a continuous pattern (see Video S2), seemingly shifting it into a "low gear." Velocity in the motility assay is believed to be limited by the rate at which myosin detaches from actin (63). This detachment rate is governed by how quickly myosin can release the diphosphate form of the substrate and then rebind a new triphosphate substrate. Therefore one or both of these parameters may be slowed with meta-AzoTP. However, the observation that the motion was continuous, combined with the observation that the V_{actin} is not increased by doubling the substrate concentration to 4 mM (see Video S7 compared with Video S2), suggests that the slowed V_{actin} is not due to a prolonged rigor state. Rather, because velocity is thought to be limited by the rate of release of the diphosphate form of the substrate at saturating substrate concentrations (74), this suggests that myosin is trapped in a state waiting for the active site to release the meta-AzoDP (Fig. 6). Thus myosin might have a very high affinity for the meta form of AzoDP, which would imply that this fast skeletal muscle myosin could be manipulated to take on the properties of a much slower myosin, such as smooth muscle myosin (59), by simply changing the isomer of the substrate. Because the structural change to the substrate is relatively minor, yet the effect on myosin is pronounced, control of the motor in this way could afford researchers with a powerful tool to gain precise detail of the mechanisms that govern, and gate, substrate binding and release from the active site. More broadly, it could be used to provide new insights into how myosin transduces chemical energy from the breakage of the gamma bond of a triphosphate-based compound into force and motion.

CONCLUSIONS

Myosin and evolutionarily related ATPases have evolved over billions of years to bind to and harness the energy of ATP hydrolysis to perform various intracellular tasks (75). Thus, it is not surprising that it has been quite challenging to develop an alternative form of energy that myosin can harness to transduce chemical energy into mechanical work as efficiently as ATP (5). Despite this challenge, we have developed an abiotic, non-nucleoside triphosphate that muscle myosin can use to drive actin filament motion (Fig. 1) and generate mechanical work (Fig. 4). Although myosin generated less force and velocity than with ATP, it is quite surprising, given the stark differences in the structure (Fig. 1), that the AzoTP can power myosin's powerstroke and cyclic interactions with an actin filament. Despite the reduced efficiency of the substrate (e.g., ortho-AzoTP versus ATP), these findings present a powerful avenue to gain control over myosin's function in two ways: first, by affecting specific steps in myosin's cross-bridge cycle, what we refer to as intrinsic control; and second, by using the light-sensitive azobenzene molecule to control by light, what we consider to be extrinsic control. This is therefore important information for ongoing efforts to gain control over molecular motors both in a cellular setting and in synthetic nanodevices. This approach will also be a powerful method to gain novel insight into the fundamental rules that govern the energy transduction process in myosin and related molecular motors.

SUPPORTING MATERIAL

Supporting Material can be found online at https://doi.org/10.1016/j.bpj.2020.06.024.

AUTHOR CONTRIBUTIONS

M.W. performed research, analyzed data, and prepared the manuscript. E.O. synthesized the reagents, performed research, and helped prepare the manuscript. S.P.J. designed and synthesized the reagents. X.L. performed research. B.S. performed research and analyzed data. M.U. performed research and analyzed data. J.C. designed research and helped write the manuscript. D.V. designed research and helped synthesize reagents and prepare the manuscript. E.P.D. designed research, performed research, analyzed data, and prepared the manuscript.

ACKNOWLEDGMENTS

This work was supported by an Innovative Project Award from the American Heart Association (grant # 18IPA34170048) to E.P.D., D.V., and J.C.

REFERENCES

1. Potma, E. J., G. J. Stienen, …, G. Elzinga. 1994. Myofibrillar ATPase activity and mechanical performance of skinned fibres from rabbit psoas muscle. *J. Physiol.* 474:303–317.
2. Brunstein, M., L. Bruno, …, V. Levi. 2009. Anomalous dynamics of melanosomes driven by myosin-V in *Xenopus laevis* melanophores. *Biophys. J.* 97:1548–1557.
3. Babkoff, A., E. Cohen-Kfir, …, S. Ravid. 2019. A direct interaction between survivin and myosin II is required for cytokinesis. *J. Cell Sci.* 132:jcs233130.
4. Abendroth, J. M., O. S. Bushuyev, …, C. J. Barrett. 2015. Controlling motion at the nanoscale: rise of the molecular machines. *ACS Nano.* 9:7746–7768.
5. Menezes, H. M., M. J. Islam, …, N. Tamaoki. 2017. Driving and photoregulation of myosin-actin motors at molecular and macroscopic levels by photo-responsive high energy molecules. *Org. Biomol. Chem.* 15:8894–8903.
6. Moussavi-Harami, F., M. V. Razumova, …, M. Regnier. 2015. 2-Deoxy adenosine triphosphate improves contraction in human end-stage heart failure. *J. Mol. Cell. Cardiol.* 79:256–263.
7. Kadota, S., J. Carey, …, G. G. Mahairas. 2015. Ribonucleotide reductase-mediated increase in dATP improves cardiac performance via myosin activation in a large animal model of heart failure. *Eur. J. Heart Fail.* 17:772–781.
8. Powers, J. D., C.-C. Yuan, …, M. Regnier. 2019. Cardiac myosin activation with 2-deoxy-ATP via increased electrostatic interactions with actin. *Proc. Natl. Acad. Sci. USA.* 116:11502–11507.
9. Chen, L., M. Nakamura, …, Z. Bryant. 2012. Engineering controllable bidirectional molecular motors based on myosin. *Nat. Nanotechnol.* 7:252–256.
10. Lindberg, F. W., M. Norrby, …, A. Månsson. 2018. Controlled surface silanization for actin-myosin based nanodevices and biocompatibility of new polymer resists. *Langmuir.* 34:8777–8784.
11. Nakamura, M., L. Chen, …, Z. Bryant. 2014. Remote control of myosin and kinesin motors using light-activated gearshifting. *Nat. Nanotechnol.* 9:693–697.
12. Schindler, T. D., L. Chen, …, Z. Bryant. 2014. Engineering myosins for long-range transport on actin filaments. *Nat. Nanotechnol.* 9:33–38.
13. ten Siethoff, L., M. Lard, …, A. Månsson. 2014. Molecular motor propelled filaments reveal light-guiding in nanowire arrays for enhanced biosensing. *Nano Lett.* 14:737–742.
14. Nicolau, D. V., Jr., M. Lard, …, D. V. Nicolau. 2016. Parallel computation with molecular-motor-propelled agents in nanofabricated networks. *Proc. Natl. Acad. Sci. USA.* 113:2591–2596.
15. Goldman, Y. E., M. G. Hibberd, and D. R. Trentham. 1984. Initiation of active contraction by photogeneration of adenosine-5′-triphosphate in rabbit psoas muscle fibres. *J. Physiol.* 354:605–624.
16. Nicolau, D. V., G. Solana, …, C. G. dos Remedios. 2007. Surface hydrophobicity modulates the operation of actomyosin-based dynamic nanodevices. *Langmuir.* 23:10846–10854.
17. Riveline, D., A. Ott, …, J. Prost. 1998. Acting on actin: the electric motility assay. *Eur. Biophys. J.* 27:403–408.
18. Svoboda, K., and S. M. Block. 1994. Force and velocity measured for single kinesin molecules. *Cell.* 77:773–784.
19. Veigel, C., J. E. Molloy, …, J. Kendrick-Jones. 2003. Load-dependent kinetics of force production by smooth muscle myosin measured with optical tweezers. *Nat. Cell Biol.* 5:980–986.
20. Tsiavaliaris, G., S. Fujita-Becker, and D. J. Manstein. 2004. Molecular engineering of a backwards-moving myosin motor. *Nature.* 427:558–561.
21. Yamada, M. D., Y. Nakajima, …, S. Maruta. 2007. Photocontrol of kinesin ATPase activity using an azobenzene derivative. *J. Biochem.* 142:691–698.
22. Smith, C. A., and I. Rayment. 1996. X-ray structure of the magnesium(II).ADP.vanadate complex of the *Dictyostelium discoideum* myosin motor domain to 1.9 A resolution. *Biochemistry.* 35:5404–5417.
23. Dantzig, J. A., J. W. Walker, …, Y. E. Goldman. 1988. Relaxation of muscle fibers with adenosine 5′-[gamma-thio]triphosphate (ATP [gamma S]) and by laser photolysis of caged ATP[gamma S]: evidence

for Ca2+-dependent affinity of rapidly detaching zero-force cross-bridges. *Proc. Natl. Acad. Sci. USA.* 85:6716–6720.

24. Gulick, A. M., C. B. Bauer, …, I. Rayment. 1997. X-ray structures of the MgADP, MgATPgammaS, and MgAMPPNP complexes of the *Dictyostelium discoideum* myosin motor domain. *Biochemistry.* 36:11619–11628.
25. Wang, D., E. Pate, …, R. Yount. 1993. Synthesis of non-nucleotide ATP analogues and characterization of their chemomechanical interaction with muscle fibres. *J. Muscle Res. Cell Motil.* 14:484–497.
26. White, H. D., B. Belknap, and W. Jiang. 1993. Kinetics of binding and hydrolysis of a series of nucleoside triphosphates by actomyosin-S1. Relationship between solution rate constants and properties of muscle fibers. *J. Biol. Chem.* 268:10039–10045.
27. Regnier, M., and E. Homsher. 1998. The effect of ATP analogs on post-hydrolytic and force development steps in skinned skeletal muscle fibers. *Biophys. J.* 74:3059–3071.
28. Regnier, M., D. M. Lee, and E. Homsher. 1998. ATP analogs and muscle contraction: mechanics and kinetics of nucleoside triphosphate binding and hydrolysis. *Biophys. J.* 74:3044–3058.
29. Nakamaye, K. L., J. A. Wells, …, R. G. Yount. 1985. 2-[(4-Azido-2-nitrophenyl)amino]ethyl triphosphate, a novel chromophoric and photoaffinity analogue of ATP. Synthesis, characterization, and interaction with myosin subfragment 1. *Biochemistry.* 24:5226–5235.
30. Pate, E., K. L. Nakamaye, …, R. Cooke. 1991. Mechanics of glycerinated muscle fibers using nonnucleoside triphosphate substrates. *Biophys. J.* 59:598–605.
31. Margossian, S. S., and S. Lowey. 1982. Preparation of myosin and its subfragments from rabbit skeletal muscle. *Methods Enzymol.* 85:55–71.
32. Debold, E. P., M. A. Turner, …, S. Walcott. 2011. Phosphate enhances myosin-powered actin filament velocity under acidic conditions in a motility assay. *Am. J. Physiol. Regul. Integr. Comp. Physiol.* 300:R1401–R1408.
33. Verdiglione, R., and M. Cassandro. 2013. Characterization of muscle fiber type in the pectoralis major muscle of slow-growing local and commercial chicken strains. *Poult. Sci.* 92:2433–2437.
34. Debold, E. P., T. J. Longyear, and M. A. Turner. 2012. The effects of phosphate and acidosis on regulated thin-filament velocity in an in vitro motility assay. *J. Appl. Physiol.* 113:1413–1422.
35. Harris, D. E., and D. M. Warshaw. 1993. Smooth and skeletal muscle myosin both exhibit low duty cycles at zero load in vitro. *J. Biol. Chem.* 268:14764–14768.
36. Ritz, C., F. Baty, …, D. Gerhard. 2015. Dose-response analysis using R. *PLoS One.* 10:e0146021.
37. Wickham, H. 2017. ggplot2: Elegant Graphics for Data Analysis. Springer-Verlag, New York.
38. Kodama, T., K. Fukui, and K. Kometani. 1986. The initial phosphate burst in ATP hydrolysis by myosin and subfragment-1 as studied by a modified malachite green method for determination of inorganic phosphate. *J. Biochem.* 99:1465–1472.
39. Longyear, T., S. Walcott, and E. P. Debold. 2017. The molecular basis of thin filament activation: from single molecule to muscle. *Sci. Rep.* 7:1822.
40. Pralle, A., M. Prummer, …, J. K. Hörber. 1999. Three-dimensional high-resolution particle tracking for optical tweezers by forward scattered light. *Microsc. Res. Tech.* 44:378–386.
41. Finer, J. T., R. M. Simmons, and J. A. Spudich. 1994. Single myosin molecule mechanics: piconewton forces and nanometre steps. *Nature.* 368:113–119.
42. Dupuis, D. E., W. H. Guilford, …, D. M. Warshaw. 1997. Actin filament mechanics in the laser trap. *J. Muscle Res. Cell Motil.* 18:17–30.
43. Guilford, W. H., D. E. Dupuis, …, D. M. Warshaw. 1997. Smooth muscle and skeletal muscle myosins produce similar unitary forces and displacements in the laser trap. *Biophys. J.* 72:1006–1021.
44. Debold, E. P., S. Walcott, …, M. A. Turner. 2013. Direct observation of phosphate inhibiting the force-generating capacity of a miniensemble of Myosin molecules. *Biophys. J.* 105:2374–2384.
45. R Core Team. 2018. R: A Language and Environment for Statistical Computing. R Foundation for Statistical Computing, Vienna, Austria.
46. Wilke, C. O. 2018. cowplot: streamlined plot theme and plot annotations for 'ggplot2'. R package version 0.9.3. https://wilkelab.org/cowplot/.
47. Brooks, B. R., R. E. Bruccoleri, …, M. Karplus. 1983. CHARMM: a program for macromolecular energy, minimization, and dynamics calculations. *J. Comput. Chem.* 4:187–217.
48. Brooks, B. R., C. L. Brooks, III, …, M. Karplus. 2009. CHARMM: the biomolecular simulation program. *J. Comput. Chem.* 30:1545–1614.
49. Huang, J., S. Rauscher, …, A. D. MacKerell, Jr. 2017. CHARMM36m: an improved force field for folded and intrinsically disordered proteins. *Nat. Methods.* 14:71–73.
50. Vanommeslaeghe, K., E. Hatcher, …, A. D. Mackerell, Jr. 2010. CHARMM general force field: a force field for drug-like molecules compatible with the CHARMM all-atom additive biological force fields. *J. Comput. Chem.* 31:671–690.
51. Fisher, A. J., C. A. Smith, …, I. Rayment. 1995. X-ray structures of the myosin motor domain of *Dictyostelium discoideum* complexed with MgADP.BeFx and MgADP.AlF4-. *Biochemistry.* 34:8960–8972.
52. Jo, S., T. Kim, …, W. Im. 2008. CHARMM-GUI: a web-based graphical user interface for CHARMM. *J. Comput. Chem.* 29:1859–1865.
53. Kim, S., J. Lee, …, W. Im. 2017. CHARMM-GUI ligand reader and modeler for CHARMM force field generation of small molecules. *J. Comput. Chem.* 38:1879–1886.
54. Darden, T., D. M. York, and L. Pedersen. 1993. Particle mesh Ewald: an N•log(N) method for Ewald sums in large systems. *J. Chem. Phys.* 98:10089–10092.
55. Ryckaert, J.-P., G. Ciccotti, and H. J. C. Berendsen. 1977. Numerical integration of the cartesian equations of motion of a system with constraints: molecular dynamics of n-alkanes. *J. Comput. Phys.* 23:327–341.
56. Robinson, D., and A. Hayes. 2018. broom: convert statistical analysis objects into tidy tibbles. https://CRAN.R-project.org/package=broom.
57. Baty, F., C. Ritz, …, M.-L. Delignette-Muller. 2015. A toolbox for nonlinear regression in R: the package nlstools. *J. Stat. Softw.* 66:1–21.
58. Leskovac, V. 2003. Comprehensive Enzyme Kinetics, 2003rd Edition. Kluwer Academic/Plenum Publishers, New York.
59. Tyska, M. J., and D. M. Warshaw. 2002. The myosin power stroke. *Cell Motil. Cytoskeleton.* 51:1–15.
60. Geeves, M. A., and K. C. Holmes. 1999. Structural mechanism of muscle contraction. *Annu. Rev. Biochem.* 68:687–728.
61. Palmiter, K. A., M. J. Tyska, …, D. M. Warshaw. 1999. Kinetic differences at the single molecule level account for the functional diversity of rabbit cardiac myosin isoforms. *J. Physiol.* 519:669–678.
62. Islam, M. J., K. Matsuo, …, N. Tamaoki. 2018. Substrate selectivity and its mechanistic insight of the photo-responsive non-nucleoside triphosphate for myosin and kinesin. *Org. Biomol. Chem.* 17:53–65.
63. Huxley, H. E. 1990. Sliding filaments and molecular motile systems. *J. Biol. Chem.* 265:8347–8350.
64. VanBuren, P., S. S. Work, and D. M. Warshaw. 1994. Enhanced force generation by smooth muscle myosin in vitro. *Proc. Natl. Acad. Sci. USA.* 91:202–205.
65. Smith, D. A., and J. Sleep. 2004. Mechanokinetics of rapid tension recovery in muscle: the Myosin working stroke is followed by a slower release of phosphate. *Biophys. J.* 87:442–456.
66. Sellers, J. R. 1999. Myosins, Second Edition. Oxford University Press, Oxford.
67. Nelson, D. L., and M. M. Cox. 2012. Lehninger Principles of Biochemistry, Second Edition. W. H. Freeman, New York.
68. Mathews, C. K., K. E. van Holde, …, S. J. Anthony-Cahill. 2012. Biochemistry, Fourth Edition. Pearson, Toronto.

69. Shaw, M. A., E. M. Ostap, and Y. E. Goldman. 2003. Mechanism of inhibition of skeletal muscle actomyosin by N-benzyl-p-toluenesulfonamide. *Biochemistry.* 42:6128–6135.

70. Ostap, E. M. 2002. 2,3-Butanedione monoxime (BDM) as a myosin inhibitor. *J. Muscle Res. Cell Motil.* 23:305–308.

71. Kovács, M., J. Tóth, …, J. R. Sellers. 2004. Mechanism of blebbistatin inhibition of myosin II. *J. Biol. Chem.* 279:35557–35563.

72. Bond, L. M., D. A. Tumbarello, …, F. Buss. 2013. Small-molecule inhibitors of myosin proteins. *Future Med. Chem.* 5:41–52.

73. Roman, B. I., S. Verhasselt, and C. V. Stevens. 2018. Medicinal chemistry and use of myosin II inhibitor (S)-Blebbistatin and its derivatives. *J. Med. Chem.* 61:9410–9428.

74. Nyitrai, M., R. Rossi, …, M. A. Geeves. 2006. What limits the velocity of fast-skeletal muscle contraction in mammals? *J. Mol. Biol.* 355:432–442.

75. Kull, F. J., R. D. Vale, and R. J. Fletterick. 1998. The case for a common ancestor: kinesin and myosin motor proteins and G proteins. *J. Muscle Res. Cell Motil.* 19:877–886.